Article

Synaptic Current Response of a Liquid Ga Electrode via a Surface Electrochemical Redox Reaction in a NaOH Solution

Dahee Seo, Heejoong Ryou, Suck Won Hong, Jong Hyun Seo, Myunghun Shin,* and Wan Sik Hwang*

ACCESS | Metrics & More | Article Recommendations

ABSTRACT: An ionic device using a liquid Ga electrode in a 1 M NaOH solution is proposed to generate artificial neural spike signals. The oxidation and reduction at the liquid Ga surface were investigated for different bias voltages at 50 °C. When the positive sweep voltage from the starting voltage (V_S) of 1 V was applied to the Ga electrode, the oxidation current flowed immediately and decreased exponentially with time. The spike and decay current behavior resembled the polarization and depolarization at the influx and extrusion of Ca^{2+} in biological synapses. Different average decay times of ∼81 and ∼310 ms were implemented for V_S of −2 and −5 V, respectively, to mimic the synaptic responses to short- and long-term plasticity; these decay states can be exploited for application in binary electrochemical memory devices. The oxidation mechanism of liquid Ga was studied. The differences in Ga ion concentration due to V_S led to differences in oxidation behavior. Our device is beneficial for the organ cell−machine interface system because liquid Ga is biocompatible and flexible; thus, it can be applied in biocompatible and flexible neuromorphic device development for neuroprosthetics, human cell−machine interface formation, and personal health care monitoring.
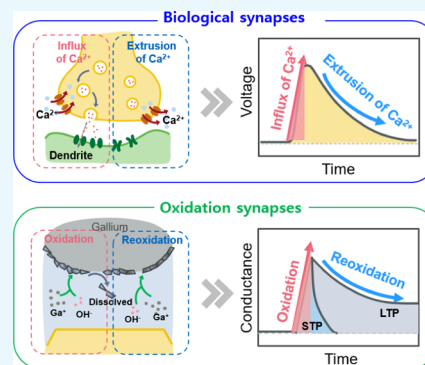
1. INTRODUCTION

With the advent of artificial intelligence (AI), learning and imitation of biological neural systems have gained considerable research interest because such systems are presumed to be the most efficient information processors conducting cognitive tasks, such as image/pattern recognition and future prediction.[1,2] The application of conventional electronics based on the von Neumann architecture is limited because of its lack of scalability and high energy consumption, as the processing and memory units are physically separated.[3,4] In contrast, biological neural systems, such as synapses, are known to consume less energy and are more efficient than any man-made electronics owing to their ability to perform parallel computing.[5] The distinct difference between biological neural systems and commercial electronics is the in-memory computing capability of biological cells, wherein information can be processed directly within the system without additional energy transfer.[6]

In biological neural systems, neurons communicate with each other via short electrical wave packets (action potentials and neural signals). Neural signals play a critical role in determining synaptic plasticity (learning and memory) in both the central nervous system (brain and spinal cord) and peripheral nervous systems (muscles and organs). Synaptic plasticity can generally be classified into two types: short-term plasticity (STP) and long-term plasticity (LTP), which are related to short- and long-term memory behaviors in psychology, respectively.[7,8] The LTP is functionally related to nonvolatile memory devices; thus, neuromorphic devices

based on LTP using phase-change memory, magneto-resistive memory, resistive random access memory, and ferroelectric random access memory have been widely investigated. In contrast, STP is useful for emulating nerves of muscles and organs that have different synaptic decay times. Thus, demonstration of synaptic signals with different decay behavior is important for the specific use of neuromorphic devices, whose behavior is similar to the Ca^{2+} dynamics in organic cells.[9,10]

Thus far, only a few studies have reported the synaptic decay characteristics, where different decay behavior was demonstrated by controlling material properties such as defects and crystallinity.[9−15] Most recent biology-inspired synaptic devices have been demonstrated to emulate the Ca^{2+} dynamics of organic cells; ion reactions were demonstrated in ion-gating synaptic transistors or liquid-based memory.[16−18] The ion- or liquid-based synaptic devices need new and diverse methods so that the electrode reliably connects the external circuit and the synaptic array, and the ionic device can be fabricated with the actual synaptic size while controlling the amount of ionic
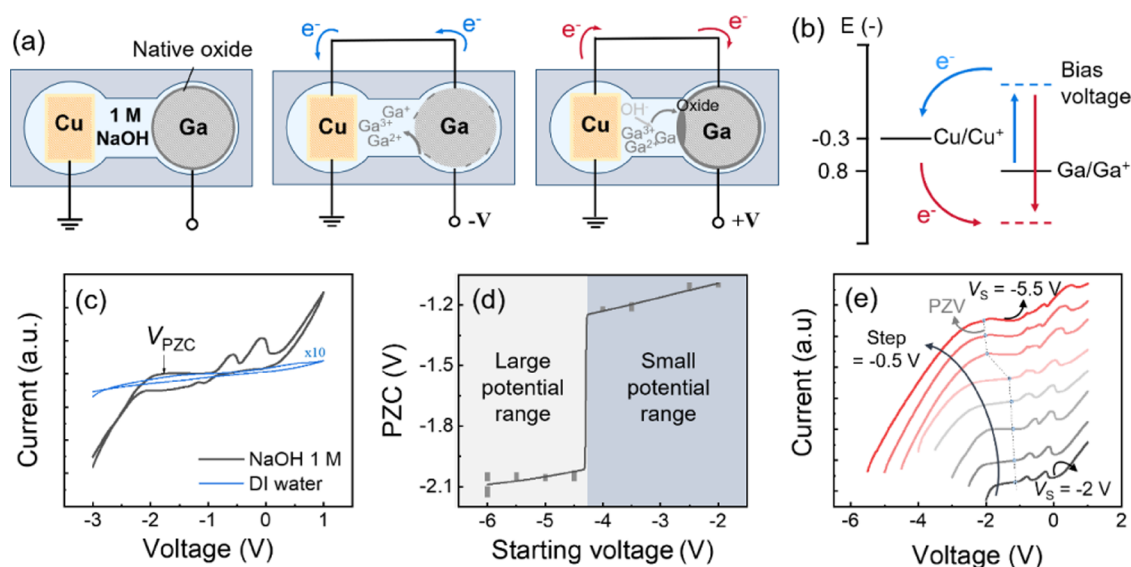
Figure 1. (a, left) Cu electrode in a cathodic reservoir is grounded. On the opposite side of the channel, the Ga electrode in the anodic reservoir was connected to the W probe. Both the reservoirs and the intermediate channel are filled with 1 M NaOH solution and are open to the air (oxygen). (a, middle) When an electrical connection is established between Ga and Cu in the 1 M NaOH solution, a spontaneous electrochemical redox reaction occurred, and this reaction becomes more favorable by applying a positive voltage at the Ga electrode. In this case, oxidation (growth of Ga oxide on the Ga electrode facing the opposite channel side) occurred at the Ga surface, while O_2 is reduced at the Cu electrode. (a, right) When a negative voltage is applied to the Ga electrode, the Ga oxide on the Ga electrode is reduced, i.e., Ga oxide is dissolved by the NaOH solution. (b) Electron energy level of Ga in respect to the Cu electrode. (c) Cyclic voltammograms of a Ga electrode in 1 M NaOH, which is compared with that in DI water. (d) Potential of zero charges (PZCs) of the Ga electrode as a function of different starting voltages in the negative region. (e) Comparison of the oxidation current of the Ga electrode with different starting voltages.

liquid. Ga is one of the abundant elements on earth, has low cost, and exhibits a stable structure when oxidized. Ga has been widely used in wide band gap oxide semiconductors for ultraviolet detection and high-voltage applications in the semiconductor industry or used in catalysts to remove volatile organic compounds in the bio-industry.[19,20] Ga can be used not only as a conductive solid electrode through a metal alloy but also as a liquid electrode in a liquid electrolyte, which provides the advantage of mechanical flexibility and biocompatibility for novel neuromorphic devices. Ga-based devices have not yet been reported to demonstrate LTP and STP in biological synapses.

In this study, we report an experimental proof of concept for generating synaptic current response and corresponding STP and LTP via surface electrochemical redox reaction at a liquid Ga electrode in a NaOH solution. We fabricated the reacting reservoir using three-dimensional (3D) printing technology to control the capacity and reaction location of Ga and electrolytes. We investigated the oxidation response of the Ga electrode and NaOH solution for different bias voltages and present the oxidation mechanism of liquid Ga, demonstrating the synaptic current responses of STP and LTP.

2. MATERIALS AND METHODS

Liquid Ga (99.999% from Sigma-Aldrich) drops (100 μL) and a Cu plate were submerged in a container of a 1 M NaOH solution (Daejung Chemicals & Metals Co.). The container was fabricated using polylactic acid using a 3D printer (FlashForge Adventurer 3); it can increase the reproducibility of the experiment with respect to the oxidation site and the amount of Ga and electrolyte used in the experiment. Ga and Cu metals function as the anode and cathode, respectively, in an open-cell, which allows atmospheric oxygen to diffuse into the NaOH solution. The Ga and Cu electrodes were separated

by 3 mm with a canal width of 1 mm. The resulting Ga electrode was in the shape of a small spherical bead with a diameter of ~1 cm. Electrical contact with Ga was established using a tungsten probe. The NaOH solution with the liquid Ga and Cu plates was heated using a hot chuck at 50 °C. The Cu plate was grounded, and a voltage was applied to the Ga electrode from −5 to 1 V using a parameter analyzer (Keithley 4200-SCS). It is noted that the liquid metal gradually moved toward the cathode when the voltage was higher than 1 V. When the voltage was less than −5 V, no significant change was observed except for the generation of gas bubbles due to the electrocatalytic water splitting.

All measurements were performed in a 1 M NaOH solution at 50 °C unless otherwise stated. The electrical synaptic responses were measured in two regimes: sweeps of a small potential range (from −2 to 1 V) and sweeps of a large potential range (from −5 to 1 V). The potential of zero charges (PZC) of the Ga electrode was extracted when the applied voltage was swept from negative to positive voltages. According to the electric double layer theory, PZC is defined as the potential (in V) at which no excess charge exists on a metal electrode.[21] Based on the PZC of the Ga electrode, the electrochemical oxidation of Ga is subjected to a change in the surface charges of the Ga electrode; a higher or lower potential than the PZC will result in the attraction of different ions on the Ga surface and eventually affect the electrochemical oxidation.

3. RESULTS AND DISCUSSION

When an ion electric channel is formed between the Ga and Cu electrodes, spontaneous half-cell reactions occur on both sides, similar to those in a galvanic cell. The Ga electrode is oxidized and releases electrons that are presumed to be consumed at the cathode side via oxygen reduction.[22] Upon

oxidation at the Ga electrode, solid Ga oxide is formed on the Ga surface, but Ga oxide can subsequently be dissolved in the NaOH solution.[22,23] It is known that Ga oxide on the Ga surface can be removed via dissolution in either low- or high-pH solution such as HCl or NaOH solution, respectively.[24] The surface reaction between the formation and dissolution of Ga oxide produces an ultrathin Ga-based oxide layer on the liquid Ga electrode under steady-state conditions. In addition to chemical removal, the Ga oxide layer can be removed electrically by applying a sufficiently negative (reducing) potential to the Ga electrode in the NaOH electrolyte. Conversely, the Ga oxide layer would be formed upon the application of a sufficiently positive (oxidizing) potential to the Ga electrode, as shown in Figure 1a,b. To investigate the growth and dissolution of the Ga oxide layer via the electrochemical reaction, cyclic voltammetry of the Ga electrode was performed in 1 M NaOH at 50 °C; the current–voltage results were compared with those in deionized (DI) water at 50 °C, as shown in Figure 1c. The potential was scanned from −3 to 1 V at 0.1 V/s and subsequently scanned reversely from 1 to −3 V. The positive potential sweeps (−3 to 1 V) revealed two anodic current peaks (oxidation peaks) when the potential was higher than −1 V, whereas the negative sweep showed a broad enhancement of the cathodic current when the applied potential was lower than −1 V. These anodic current peaks were attributed to the formation of gallium oxide on the gallium surface, while the broad enhancement of the cathodic current was presumably attributed to the reduction of the dissolved oxygen near the Cu cathode electrode rather than Ga deposition.[23,25] As expected, no noticeable faradaic and non-faradaic charging currents were observed with the DI water at 50 °C, as shown in Figure 1c. This indicates that electrochemical reactions occurred on the Ga surface via either oxidation or reduction in the 1 M NaOH solution at 50 °C.

The PZC was measured for the positive potential sweep while maintaining the ending voltage (1 V) and changing the starting voltage (V_S) of the sweep (V_S to 1 V). The PZC values decreased linearly with the decrease in the starting potential; however, the values decreased rapidly near $V_S = −4$ V, as shown in Figure 1d. Interestingly, Figure 1d shows that there are two distinct states in Ga oxidation that are distinguishable based on the starting potential: a wide potential range ($V_S < −4$ V) and a narrow potential range ($V_S ≥ −4$ V). Figure 1e exhibits the oxidation current of the Ga electrode with different V_S values. At V_S from −2.0 to −4.0 V, two oxidation peaks were observed,[23] while additional peaks were observed when the V_S values changed from −4.5 to −5.5 V. It is known that the most stable ion of Ga is Ga^{3+} by losing three electrons; thus, three oxidation reactions are expected during the positive potential sweep; each electron transfer process is Ga to Ga^+, Ga^+ to Ga^{2+}, and Ga^{2+} to Ga^{3+}.[24]

The typical oxidation process in each group can be analyzed using the oxidation current, as shown in Figure 2. Figure 2a illustrates the oxidation current for the sweep at V_S of −2 and −5 V; the result at $V_S = −2$ V was similar to the results at V_S of −2.5, −3.0, −3.5, or −4.0 V, while the results at $V_S = −5$ V were similar to those at V_S of −4.5 or −5.5 V. The current shape with $V_S = −2$ V exhibiting two prominent oxidation peaks was consistent with previous studies.[24,26] The first peak in the low-voltage region (LVR) was attributed to a two-step electron transfer process (Ga to Ga^+ and Ga^+ to Ga^{2+}), and the second peak in the high-voltage region (HVR) is known to represent the final oxidation step (Ga^{2+} to Ga^{3+}, Ga^+ to Ga^{3+},
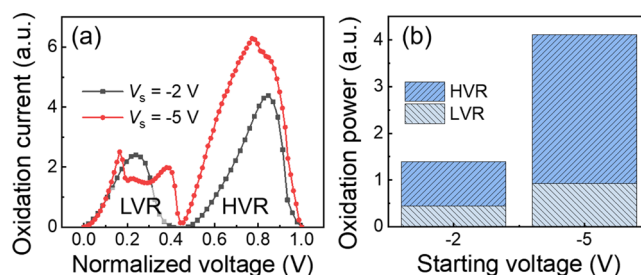
Figure 2. (a) Oxidation current at the starting voltage (V_S) of −2 and −5 V. Background current was subtracted using the linear method. The low-voltage region (LVR) and high-voltage region (HVR) represent the different oxidation states caused by the low-voltage and high-voltage ranges, respectively. (b) Comparison of the oxidation power, including the LVR and HVR at different V_S, where the oxidation power is the product of voltage and current.

and Ga to Ga^{3+}).[23,26] In contrast, different peak shapes and peak areas were observed at $V_S = −5$ V. Figure 2b compares the oxidation power that is a product of the applied voltage and the oxidation current, which indicates the absorbed energy during the oxidation process. The oxidation power at $V_S = −5$ V was much higher than that at $V_S = −2$ V. It is noteworthy that considering the Gaussian-like shapes of LVR at $V_S = −2$ V (Figure 2a), the irregular shapes of LVR at $V_S = −5$ V (Figure 2a) can be seen presumably due to the repetition of the dissolution and oxidation, which would be further discussed with Figure 4a,b. These differences indicate that the electrochemical reaction in the Ga surface was different based on the V_S value, although the ending voltage was 1 V in both cases.

To further investigate the transient current, the step response of the oxidation current was measured. For the step response measurements, the voltage of the Ga electrode was changed from V_S to 1 V, and the results were compared for different V_S values of −2 and −5 V. Figure 3a,b shows the
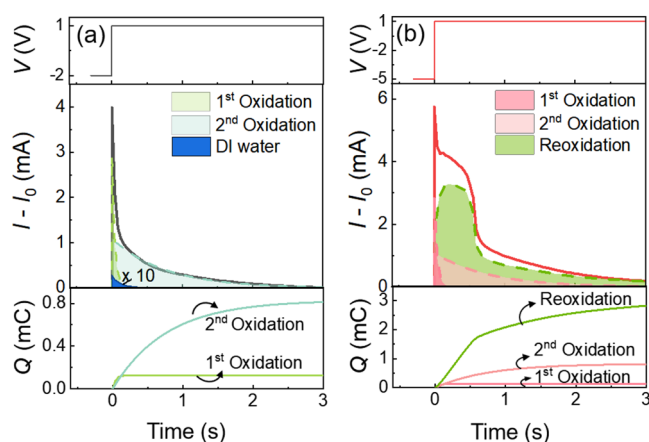
Figure 3. Step response of oxidation current and total electric charges (Q, obtained by integrating the oxidation current over time) when the Ga potential of a unit step function is applied for V_S of (a) −2 V for one-time oxidation and (b) −5 V for extended oxidation.

transient current response at the moment of the positive potential sweep for the Ga surface at $V_S = −2$ V and $V_S = −5$ V, respectively. When the voltage changed from −2 to 1 V, electrochemical oxidation occurred, resulting in the immediate formation of Ga oxide on the Ga surface, which contributed to the initial spike current component. Once the Ga oxide layer
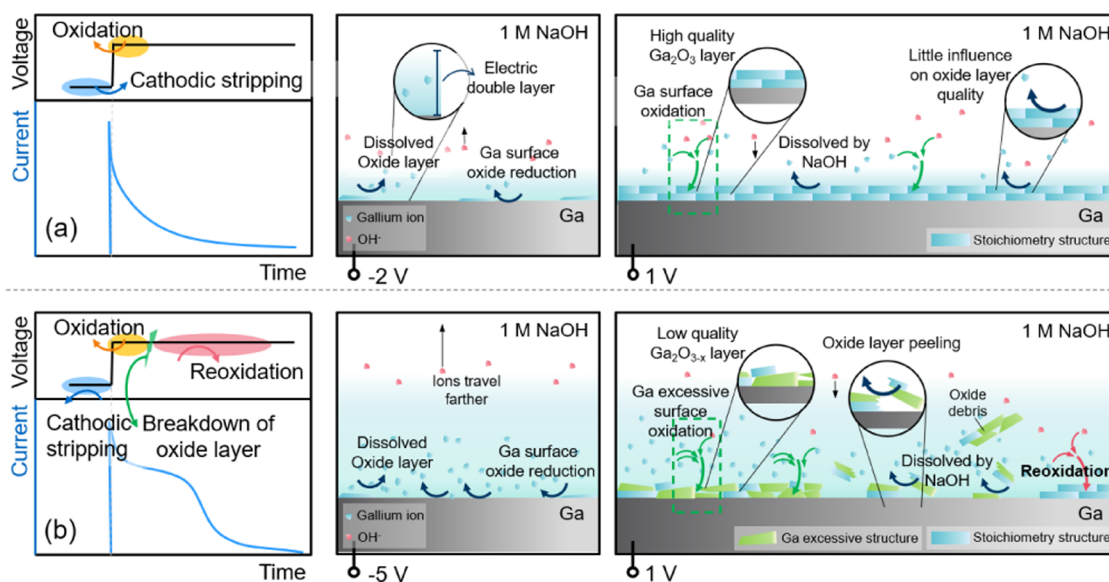
Figure 4. Schematic illustration of the proposed oxidation mechanism under different conditions of V_S at (a) −2 V and (b) −5 V.
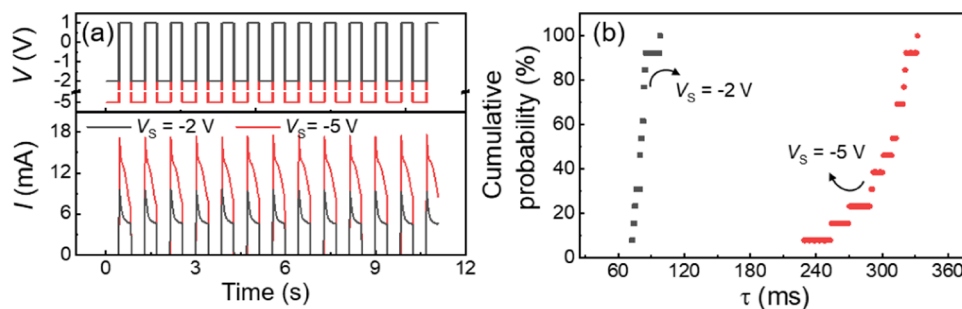
Figure 5. (a) Generating of synaptic spike responses using voltage pulsation and (b) cumulative probability of Ga-based neuromorphic devices at V_S of −2 and −5 V.

was formed, it prevented further oxidation reactions on the Ga surface; hence, the oxidation current decreased exponentially with time and finally reached a stable current, and it was named "one-time oxidation" in Figure 3a because the oxidation process takes place all at once. The current-spike and decay behavior in the liquid Ga system resembles the polarization and depolarization processes owing to the influx and extrusion of Ca^{2+} in biological synapses. The current decay characteristic of the Ga surface at $V_S = -2$ V was fitted using two exponential functions that presumably present two oxidation processes presenting 1st and 2nd oxidation current components, respectively, as in eq 1.

$$I = I_0 + I_1 \exp\left(-\frac{t}{\tau_1}\right) + I_2 \exp\left(-\frac{t}{\tau_2}\right) \quad (1)$$

where I_0 is the saturation current, I_1 ($\cong 0.0029$) and I_2 ($\cong 0.0011$) are the pre-factors, and τ_1 ($\cong 0.04$) and τ_2 ($\cong 0.76$) are each decay constants representing the growth speed of the oxide layer. For comparison, an identical system was tested in DI water instead of NaOH solution. The measured current in DI water was negligible compared to that in the NaOH solution, as shown in Figure 3a, which indicates that no oxidation reaction occurred on the Ga surface in DI water.

On the other hand, the current decay characteristics of the Ga surface at $V_S = -5$ V were more complex than those at $V_S =$

−2 V. The condition in Figure 3a exhibited a fast decay characteristic (∼81 ms), while that in Figure 3b showed a slow decay characteristic (∼310 ms). The different decay behaviors at $V_S = -2$ V and $V_S = -5$ V could be explained by the difference in oxidation mechanisms, as shown in Figure 4. The additional reoxidation process resulting in the slow decay characteristic at $V_S = -5$ V was presumably attributed to the repetition of the dissolution and oxidation. It is noteworthy that, as observed in Figures 1 and 2, the current response can also be classified into two groups. Figure 3a,b shows the typical behavior of each group.

Figure 4 illustrates a schematic drawing of the proposed oxidation mechanism at $V_S = -2$ V and $V_S = -5$ V, showing the different behaviors of reduction/dissolution and oxidation at the Ga surface. For $V_S < -1$ V, the Ga oxide layer on the Ga electrode is reduced and dissolved, which changed the concentration of ions in the electric double layer at the liquid Ga and NaOH interface. The concentration of Ga ions near the Ga surface was much higher at $V_S = -5$ V than at $V_S = -2$ V because the ion drift force was stronger at higher electric fields. When the voltage changed from −2 to 1 V, it was presumed that the electric double layer with the low Ga ion concentration would be easily oxidized to form a stoichiometric Ga_2O_3 layer. The formed stoichiometric Ga_2O_3 layer might be stable and robust in the NaOH solution, which prevented further oxidation reactions from penetrating liquid Ga; it resulted in the fast decay behavior of one-time oxidation,
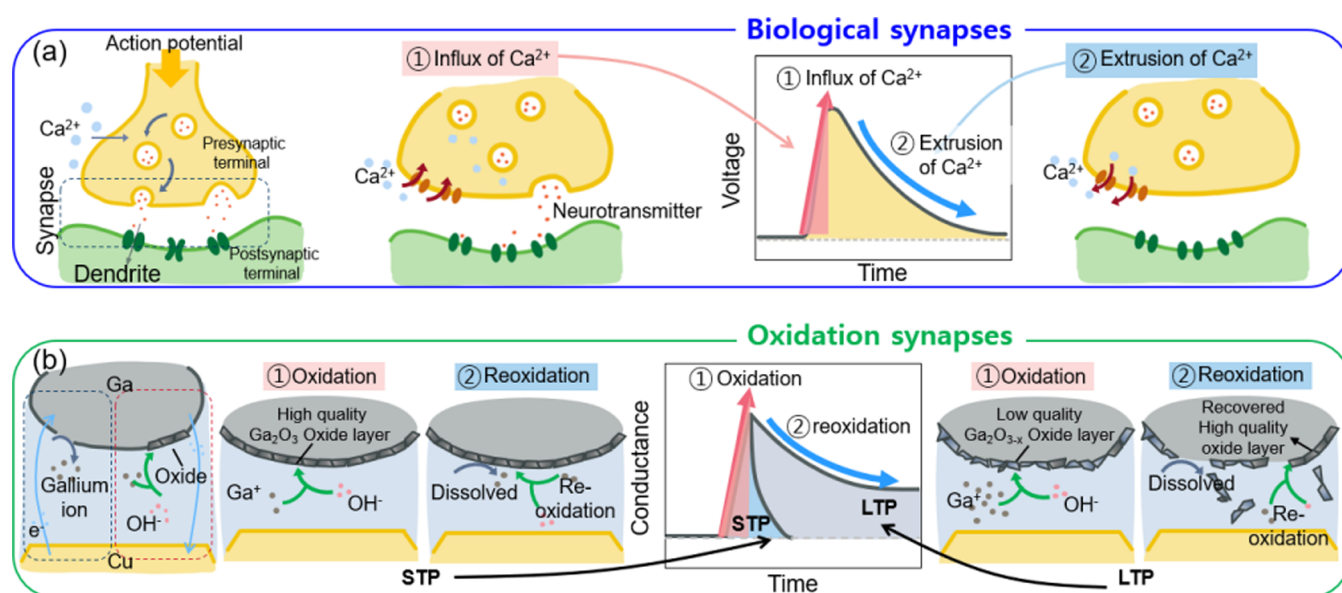
Figure 6. Schematic of (a) biological synapses caused by the influx and extrusion process of Ca^{2+} in the cell and (b) redox synapses caused by oxidation current.
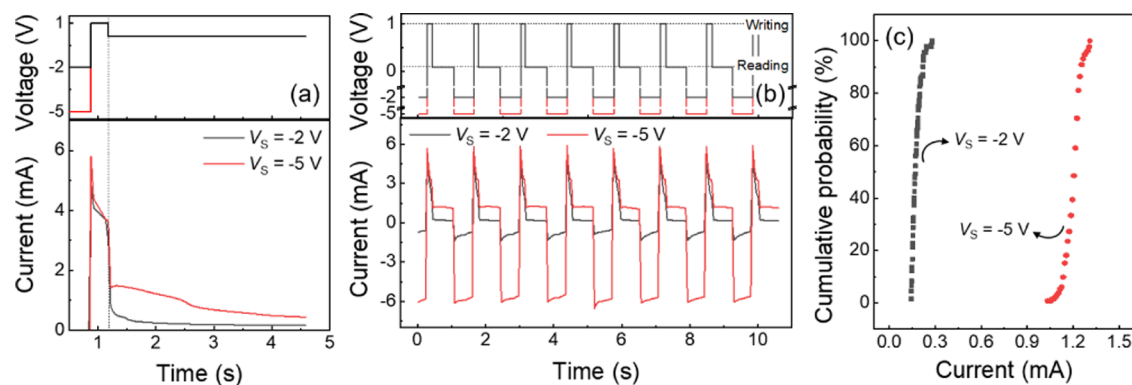
Figure 7. (a) Spike−response characteristics of the Ga-based device at different V_S values. (b) Cycle test results and (c) cumulative probability of two typical spike responses at V_S of −2 and −5 V for a long-term persistent storage application.

as shown in Figure 3a. In contrast, when the voltage changed from −5 to 1 V, the electric double layer with the excessive Ga ions was presumed to form a mixture of stoichiometric Ga_2O_3 layer and Ga oxide layer in excess of Ga or O-deficient, as shown in Figure 4b. This mixed layer would be unstable and easily soluble in the NaOH solution, thereby forming pits, pinholes, and microcrevices owing to mechanical cracking and stress between liquid Ga and NaOH solution. Therefore, when the voltage changes from −5 to 1 V, an initial oxidation reaction takes place on the entire surface at first, but soon parts of the nonuniform and unstable Ga oxide layer separate into solution and dissolve, where new oxidation begins locally again; the dissolution and oxidation occur randomly and partially on the Ga oxide surface and continue over time until the entire surface is covered with stoichiometric Ga_2O_3. The reoxidation current response of Figure 3b is attributed to the occurrence and decaying of the 1st and 2nd oxidation currents continuously over time in accordance with the dissolution of the Ga oxide layer; it is the slow decay behavior, named "extended oxidation" in Figure 3b.

The overall synaptic spike response generated with the voltage pulsation is shown in Figure 5a; the fast and slow decay behaviors are well compared. In this study, the effective decay

time (τ) is defined as the time required to reach ∼37% ($\cong e^{-1}$) of the initial current. The average decay time for the fast decay condition was ∼81 ms, while that for the slow decay condition was ∼310 ms. Figure 5b shows the cumulative probability of each decay time under different conditions. The results showed that the fast and slow decay behaviors were distinguished and can be used as spiking signals for neuromorphic devices. The spiking and decaying current behaviors are very similar to the polarization and depolarization processes caused by the influx and extrusion process of Ca^{2+} in organic cells, as shown in Figure 6. In addition, these different current decaying behaviors have often been observed and studied in the field of oxide semiconductors, where the PPC effect is involved.

Figure 7 shows a long-term persistent storage application using a liquid Ga electrode. Unlike the measurement conditions in Figures 3−5, the voltage was swept from V_S to 1 V, kept at 1 V for 10 s, and subsequently reduced by 0.1 V for the current reading. The voltage was maintained at 0.1 V for 3 s, then returned to the original V_S and maintained for 4 s. While this sequence (Figure 7a) was repeated, the current spikes exhibited two periodic patterns for the V_S values, which showed two different current states at 0.1 V, as shown in Figure 7b. The average current values of the current for the Ga

system with V_S of −2 and −5 V were 0.17 and 1.2 mA, respectively. The current was altered by approximately 10 times at V_S of −2 and −5 V. This Ga system demonstrated a decent and stable cycling performance and cumulative probability, as shown in Figure 7b,c, respectively.

4. CONCLUSIONS

An experimental proof of concept for the current−spike response and corresponding STP and LTP was demonstrated via a surface electrochemical redox reaction at a liquid Ga electrode in a NaOH solution. The current−spike and decay behavior in this work resembled the polarization and depolarization processes owing to the influx and extrusion of Ca^{2+} in biological synapses. By controlling the oxidation reaction at the liquid Ga surface, different decay behaviors of STP and LTP were demonstrated. The average decay time for the fast decay condition was ∼81 ms, while that for the slow decay condition was ∼310 ms. The decay time difference could also be used for binary memory devices; the average current values for the Ga system with V_S of −2 and −5 V were 0.17 and 1.2 mA, respectively. The proposed liquid Ga-electrode-based neuromorphic device could be implemented in the interface system between organ cells and machines as liquid Ga is biocompatible and flexible. Our results mark a step toward the development of biocompatible and flexible neuromorphic devices for neuroprosthetics, the formation of human cell−machine interfaces, and personal health care monitoring.

■ AUTHOR INFORMATION

Corresponding Authors

Myunghun Shin − *School of Electronics and Information Engineering, Korea Aerospace University, Goyang 10540, Republic of Korea*; Email: mhshin@kau.ac.kr

Wan Sik Hwang − *Department of Materials Science and Engineering, Korea Aerospace University, Goyang 10540, Republic of Korea; Smart Drone Convergence, Korea Aerospace University, Goyang 10540, Republic of Korea*; ⊙ orcid.org/0000-0002-0060-9348; Email: whwang@kau.ac.kr

Authors

Dahee Seo − *Department of Materials Science and Engineering, Korea Aerospace University, Goyang 10540, Republic of Korea; Smart Drone Convergence, Korea Aerospace University, Goyang 10540, Republic of Korea*

Heejoong Ryou − *Department of Materials Science and Engineering, Korea Aerospace University, Goyang 10540, Republic of Korea*

Suck Won Hong − *Department of Cogno-Mechatronics Engineering, Department of Optics and Mechatronics Engineering, Pusan National University, Busan 46241, Republic of Korea*; ⊙ orcid.org/0000-0001-7291-1020

Jong Hyun Seo − *Department of Materials Science and Engineering, Korea Aerospace University, Goyang 10540, Republic of Korea*

Complete contact information is available at:
https://pubs.acs.org/10.1021/acsomega.2c01645

Notes

The authors declare no competing financial interest.

■ REFERENCES

(1) Abiodun, O. I.; Jantan, A.; Omolara, A. E.; Dada, K. V.; Mohamed, N. A.; Arshad, H. State-of-the-art in artificial neural network applications: A survey. *Heliyon* **2018**, *4*, No. e00938.

(2) Alzubaidi, L.; Zhang, J.; Humaidi, A. J.; Al-Dujaili, A.; Duan, Y.; Al-Shamma, O.; Santamaría, J.; Fadhel, M. A.; Al-Amidie, M.; Farhan, L. Review of deep learning: Concepts, CNN architectures, challenges, applications, future directions. *J. Big Data* **2021**, *8*, 53.

(3) Ielmini, D.; Ambrogio, S. Emerging neuromorphic devices. *Nanotechnology* **2020**, *31*, No. 092001.

(4) Zhang, W.; Gao, B.; Tang, J.; Yao, P.; Yu, S.; Chang, M.; Yoo, H.; Qian, H.; Wu, H. Neuroinspired computing chips. *Nat. Electron.* **2020**, *3*, 371−382.

(5) Marković, D.; Mizrahi, A.; Querlioz, D.; Grollier, J. Physics for neuromorphic computing. *Nat. Rev. Phys.* **2020**, *2*, 499−510.

(6) Wong, H. S.; Salahuddin, S. Memory leads the way to better computing. *Nat. Nanotechnol.* **2015**, *10*, 191−194.

(7) Kim, M. K.; Lee, J. S. Short-term plasticity and long-term potentiation in artificial biosynapses with diffusive dynamics. *ACS Nano* **2018**, *12*, 1680−1687.

(8) Pfister, J. P.; Lengyel, M. Interactions between short-term and long-term plasticity: shooting for a moving target. *Nat. Prec.* **2011**, DOI: 10.1038/npre.2011.5857.1.

(9) Go, G.-T.; Lee, Y.; Seo, D.; Pei, M.; Lee, W.; Yang, H.; Lee, T. Achieving microstructure-controlled synaptic plasticity and long-term retention in ion-gel-gated organic synaptic transistors. *Adv. Intell. Syst.* **2020**, *2*, No. 2000012.

(10) Seo, D.-G.; Lee, Y.; Go, G.; Pei, M.; Jung, S.; Jeong, Y. H.; Lee, W.; Park, H.; Kim, S.; Yang, H.; Yang, C.; Lee, T. Versatile neuromorphic electronics by modulating synaptic decay of single organic synaptic transistor: From artificial neural networks to neuroprosthetics. *Nano Energy* **2019**, *65*, No. 104035.

(11) Ke, Y.; Yu, R.; Lan, S.; He, L.; Yan, Y.; Yang, H.; Shan, L.; Chen, H.; Guo, T. Polymer bulk-heterojunction synaptic field-effect transistors with tunable decay constant. *J. Mater. Chem. C* **2021**, *9*, 4854−4861.

(12) Tang, B.; Hussain, S.; Xu, R.; Cheng, Z.; Liao, J.; Chen, Q. Novel type of synaptic transistors based on a ferroelectric semiconductor channel. *ACS Appl. Mater. Interfaces* **2020**, *12*, 24920−24928.

(13) Duan, H.; Liang, L.; Wu, Z.; Zhang, H.; Huang, L.; Cao, H. IGZO/CsPbBr3-Nanoparticles/IGZO neuromorphic phototransistors and their optoelectronic coupling applications. *ACS Appl. Mater. Interfaces* **2021**, *13*, 30165−30173.

(14) Kim, M. K.; Lee, J. S. Synergistic improvement of long-term plasticity in photonic synapses using ferroelectric polarization in Hafnia-based oxide-semiconductor transistors. *Adv. Mater.* **2020**, *32*, No. 1907826.

(15) Wang, Y.; Yin, L.; Huang, W.; Li, Y.; Huang, S.; Zhu, Y.; Yang, D.; Pi, X. Optoelectronic synaptic devices for neuromorphic computing. *Adv. Intell. Syst.* **2021**, *3*, No. 2000099.

(16) Nikam, R. D.; Kwak, M.; Lee, J.; Rajput, K. G.; Banerjee, W.; Hwang, H. Near ideal synaptic functionalities in Li ion synaptic transistor using $Li_3PO_xSe_x$ electrolyte with high ionic conductivity. *Sci. Rep.* **2019**, *9*, No. 18883.

(17) Park, Y.; Kim, M.-K.; Lee, J.-S. Ion-gating synaptic transistors with long-term synaptic weight modulation. *J. Mater. Chem. C* **2021**, *9*, 5396−5402.

(18) Kim, D.; Lee, J.-S. Designing artificial sodium ion reservoirs to emulate biological synapses. *NPG Asia Mater.* **2020**, *12*, 62.

(19) Ryou, H.; Yoo, T. H.; Yoon, Y.; Lee, I. G.; Shin, M.; Cho, J.; Cho, B. J.; Hwang, W. S. Hydrothermal synthesis and photocatalytic

property of Sn-doped β-Ga2O3 nanostructure. *ECS J. Solid State Sci. Technol.* **2020**, *9*, No. 045009.

(20) Han, Z.; Liang, H.; Huo, W.; Zhu, X.; Du, X.; Mei, Z. Boosted UV photodetection performance in chemically etched amorphous Ga$_2$O$_3$ thin-film transistors. *Adv. Opt. Mater.* **2020**, *8*, No. 1901833.

(21) Le, J.; Iannuzzi, M.; Cuesta, A.; Cheng, J. Determining potentials of zero charge of metal electrodes versus the standard hydrogen electrode from density-functional-theory-based molecular dynamics. *Phys. Rev. Lett.* **2017**, *119*, No. 016801.

(22) Gough, R. C.; Dang, J. H.; Moorefield, M. R.; Zhang, G. B.; Hihara, L. H.; Shiroma, W. A.; Ohta, A. T. Self-actuation of liquid metal via redox reaction. *ACS Appl. Mater. Interfaces* **2016**, *8*, 6−10.

(23) Perkins, R. S. Anodic oxidation of gallium in alkaline solution. *J. Electroanal. Chem. Interfacial Electrochem.* **1979**, *101*, 47−57.

(24) Song, M.; Daniels, K. E.; Kiani, A.; Rashid-Nadimi, S.; Dickey, M. D. Interfacial tension modulation of liquid metal via electrochemical oxidation. *Adv. Intell. Syst.* **2021**, *3*, No. 2100024.

(25) Chung, Y.; Lee, C. W. Electrochemistry of Gallium. *J. Electrochem. Sci. Technol.* **2013**, *4*, 1−18.

(26) Steichen, M.; Thomassey, M.; Siebentritt, S.; Dale, P. J. Controlled electrodeposition of Cu−Ga from a deep eutectic solvent for low cost fabrication of CuGaSe 2 thin film solar cells. *Phys. Chem. Chem. Phys.* **2011**, *13*, 4292−4302.